Journal Pre-proof

The effect of near-surface plastic deformation on the hot corrosion and high temperature corrosion-fatigue response of a nickel-based superalloy

H.L. Cockings, B.J. Cockings, W. Harrison, M. Dowd, K.M. Perkins, M.T. Whittaker, G.J. Gibson

PII: S0925-8388(20)31252-4

DOI: https://doi.org/10.1016/j.jallcom.2020.154889

Reference: JALCOM 154889

To appear in: *Journal of Alloys and Compounds*

Received Date: 14 January 2020

Revised Date: 28 February 2020

Accepted Date: 20 March 2020

Please cite this article as: H.L. Cockings, B.J. Cockings, W. Harrison, M. Dowd, K.M. Perkins, M.T. Whittaker, G.J. Gibson, The effect of near-surface plastic deformation on the hot corrosion and high temperature corrosion-fatigue response of a nickel-based superalloy, *Journal of Alloys and Compounds* (2020), doi: https://doi.org/10.1016/j.jallcom.2020.154889.

CRediT author statement

Dr Hollie Cockings
Conceptualization, methodology, validation, formal analysis, investigations, writing, visualisation.

Dr Benjamin Cockings
Validation, formal analysis, investigation, data curation.

Dr Will Harrison
Methodology, software, formal analysis.

Dr Michael Dowd
Conceptualization, investigation.

Dr Karen Perkins
Conceptualization, supervision, project administration and funding acquisition.

Dr Mark Whittaker
Supervision, writing – review & editing, validation.

Dr Grant Gibson
Conceptualization, resources, project administration.

The effect of near-surface plastic deformation on the hot corrosion and high temperature corrosion-fatigue response of a nickel-based superalloy

H.L.Cockings[1*], B.J.Cockings[2], W.Harrison[1], M.Dowd[1], K.M.Perkins[1], M.T. Whittaker[2], G.J.Gibson[3]

[1] Materials Research Centre, College of Engineering, Swansea University, Swansea, SA1 8EN, UK

[2] Institute of Structural Materials, Swansea University, Swansea, SA1 8EN, UK

[3] Rolls-Royce plc, Derby, P.O.Box 31, DE24 8BJ, UK

*Corresponding author: H.L.Cockings@swansea.ac.uk, +44 1792 604719

Keywords: high-temperature alloys; surfaces and interfaces; corrosion; oxidation; microstructure; mechanical properties

Abstract

Surface treatments such as shot peening to inhibit fatigue crack initiation are essential processes when designing gas turbine components for aerospace applications. It is therefore crucial to understand the effects of shot peening in representative service environments. Here, the influence of surface treatment on the high temperature corrosion fatigue response of a polycrystalline nickel-based superalloy is considered, an area that has not previously been explored. Two shot peening conditions; 110H 7A 200% and 330H 7A 200%, along with a polished surface were chosen. Specimens were salted and exposed to SO_2 gas during fatigue testing at 700°C. A range of novel techniques including SEM, EBSD and axial chromatism profilometry were used to analyse the near surface cold work and surface condition before and after testing. EBSD local misorientation maps, paired with an increase in corrosion-fatigue life, suggest that a greater depth of cold work produced by the smaller shot size (110H), is providing a significant benefit in terms of hot corrosion and corrosion-fatigue performance. This paper concludes that the presence of a substantial layer of cold work is required to account for any metal loss due to the effects of hot corrosion. It is also evident that cold work hinders fatigue crack initiation and delays the onset of pit to crack transition.

1. Introduction

As gas turbine operating temperatures increase due to the demand for higher engine efficiencies, the propensity for hot corrosion and high temperature corrosion-fatigue also increases. Hot corrosion is a mechanism of accelerated attack which can occur when an alloy is exposed to sulfur bearing gases and salts at elevated temperatures. Two types of hot corrosion are commonly discussed within the literature; Type I and Type II. Type I hot corrosion, also known as *high temperature hot corrosion* typically takes place in the temperature range of 800-950˚C and is attributed to the failure of surface oxide scale. Type II, commonly known as *low temperature hot corrosion,* on the other hand, takes place in the range of 650-800˚C, which is more akin to the operating temperatures of the turbine disc. A significant partial pressure of SO_3 is required to generate the Type II mechanism, which occurs due to the combination of SO_2 and O_2. The initial oxidation of nickel to form NiO may also

behave as a catalyst, increasing the partial pressure of SO_3. The combination of NiO and SO_3 converts solid Na_2SO_4 to a liquid (molten) solution of Na_2SO_4 – $NiSO_4$ [1]. It has been proposed that the SO_3 is then transported through the Na_2SO_4 – $NiSO_4$ phase to the liquid-substrate interface and at this point, Ni ions will diffuse and precipitate out into the liquid sulfate. The dissolution of Ni from the alloy causes any Cr_2O_3 and Al_2O_3 protective scales to become discontinuous or non-protective [2]. Type II hot corrosion is commonly accompanied by pitting or broad-front attack, with little to no internal sulfidation damage [3]. Viswanathan describes the characteristic features of Type II hot corrosion to consist of a non-protective outer NiO scale, with an inner, mixed Cr, Al oxide scale. A sulfur rich layer also sits between the oxide and the metal substrate, which will occur during the transportation of SO_3 through the liquid phase [4]. When combined with a cyclic stress, Type II hot corrosion becomes *high temperature corrosion-fatigue*, which, until recently, was not fully understood. The recent development of a novel test capability, where representative service environments have been simulated via the combined exposure of specimens to sulfuric gases, salts and a cyclic waveform, has enabled a fundamental understanding of the high temperature corrosion-fatigue mechanism in polycrystalline Ni-alloys [5]. This work has shown that the combined effect of corrosion and fatigue will result in an, as expected, reduction in fatigue life when compared with air-only exposure. The Type II hot corrosion mechanism, however, is enhanced with the addition of internal grain boundary attack in the form of Ti and Cr sulfide particles, ahead of the advancing oxide front. It is believed that this is attributed to the localised rupture of oxide scales and the de-cohesion of grain boundaries, due to a sufficient stress amplitude, resulting in the inward diffusion of sulfur into the bulk matrix. This, in due course, will result in the formation of a stress raising feature such as a pit or a 'V' shaped channel, where a fissure or fatigue crack could initiate.

Shot peening has historically been utilised as a method of surface treatment for critical rotating parts within the gas turbine, to prevent the initiation of fatigue cracks. The free surface of a material is a common site for the nucleation and initiation of fatigue cracks due to the propensity for surface damage and the lack of surface constraint at a microstructural level [6]. Shot peening is carried out by imparting small spherical media (cast steel or glass) to the component or sample at high velocities, which will induce a layer of compressive residual stress (CRS) and plastic deformation at the surface. It is believed that the CRS will reduce the effect of externally applied tensile loads, thus improving the crack growth resistance of the material. Evans *et al*, as well as a number of others, have shown, however, that following thermal exposure and/or mechanical loading, the advantages of CRS are diminished, and residual stresses become relaxed [7].

Recent studies [5][8] have discussed that there is a possible relationship between the mechanism of hot corrosion and the surface condition due to shot peening. This paper aims to investigate this relationship and explore the effect of surface roughness and cold work on the corrosion-fatigue life in a nickel-based superalloy.

2. Material and Methods

2.1. Material and Specimens

All testing was carried out on nickel-based superalloy, fine grain RR1000. RR1000 is a high strength, high temperature capability, powder metallurgy alloy manufactured specifically for disc rotor applications within the gas turbine engine. The alloy consists of a γ matrix with an average grain size of 8μm and γ′ precipitates Ni_3 (Al, Ti, Ta), as shown in Figure 1. The chemical composition is shown in Table 1 [9].

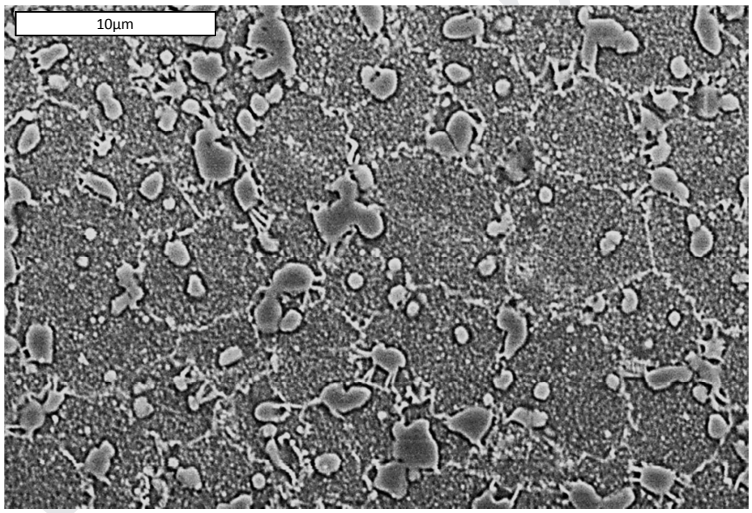

Figure 1 – SEM micrograph of alloy RR1000, etched with Kallings Reagent

Co	Cr	Mo	Ti	Al	Ta	Hf	C	B	Zr	Ni
18.5	15	5	3.6	3	2	0.5	0.03	0.02	0.06	Bal

Table 1 - %wt composition of RR1000 [9]

Two specimen types were provided for this study; flat plate samples for static hot corrosion testing (10x10x5mm) and round bar specimens with a 9mm diameter, for dynamic high temperature corrosion-fatigue testing, shown in Figure 2a and 2b.

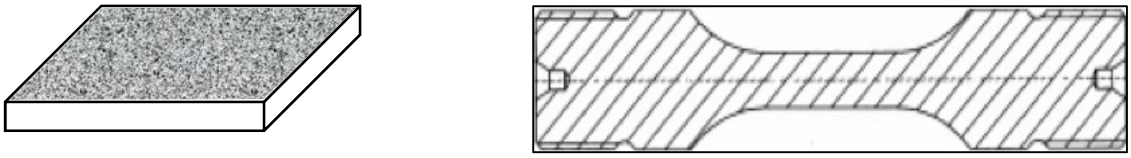

(a) (b)

Figure 2 – Fine grain RR1000 test specimens (a) Flat plate specimen, (b) Round bar fatigue specimen

All specimen surfaces were shot peened in accordance with AMS2432 [10] utilising a robotic setup with a ½" nozzle. Cast steel media were used with a fixed intensity of 7 Almen (+/- 0.5A) and coverage of 200%. Two shot sizes were utilised per sample for comparison; 110H and 330H, all other peening variables remained fixed. Fatigue specimens were also provided in the un-peened condition and polished to a 1µm surface finish to allow for baseline fatigue data to be generated, without the influence of surface treatment.

2.2 Analysis and Material Preparation Techniques

The surface roughness of each peened condition was measured by scanning four separate areas, pre and post-test, with a surface profilometer to determine an average value for S_a. A Nanovea PS50, which uses axial chromatism, was employed to scan the surface. Axial chromatism based techniques work on the principle that each separate wavelength of a white light source will have different focal lengths, thus allowing a single chromatic point to always be in focus. Only the wavelength that is in focus can pass through a spatial filter thus allowing a measurement to be taken. Once the surface was scanned, Mountains Ultra software was utilised to analyse the surface data. Non-measured points were removed, and a Robust Gaussian filter was applied to the data in accordance with ISO 16610-71 to distinguish roughness from waviness [11]. Values for S_a could then be calculated using equation 1;

$$S_a = \frac{1}{A}\int |z(x,y)|dxdy \qquad \text{(Equation 1)}$$

Since the use of R_a (arithmetical mean height of a line) is a historically well-established technique of determining surface roughness, a number of line scans were also conducted to allow for a direct comparison with S_a (arithmetical mean height of an area) and to ensure consistency when comparing with previous literature [12]. Values for R_a were measured by

taking 10 horizontal line scans at equal distances across the 4x4mm measured area. Equation 2 was then used to calculate Ra values, with an average being used for the final result. The function lb is the sample length and Z(x) is the profile height function.

$$R_a = \frac{1}{lb}\sum_{0}^{lb} |\, Z\,(x)|$$

(Equation 2)

Following exposure to a corrosive environment, before post-test profilometry was conducted, the samples were cleaned in an ultrasonic bath using a neutral cleaning agent in order to assess the physical damage to the metal substrate. Sa measurements were obtained to allow for an accurate representation of corrosion damage across a 4x4mm surface area. When determining pit depth and pit density, depth constitutes as the measurement between a plane that approximates the average elevation from the rim around a pit and the deepest point within the pit. The pit rim is defined by a saddle point, were the slope of the pit in orthogonal directions is equal to zero.

For this study, an EBSD kernel average misorientation (KAM) approach has been used to determine the depth of near-surface plastic deformation. As shot peening induces plastic strain into the near surface, and plastic strain is localised distortion of the crystal lattice, a layer of low angle local misorientation can be observed on the surface of the treated material. This method allows for a greater accuracy as the local misorientations are calculated on a pixel to pixel bases rather than being averaged for the whole grain [13][14]. To prepare for EBSD analysis, specimens were first cross-sectioned using a Struers Setocom 10 cutting wheel utilising a slow feed speed and wheel speed to ensure no additional heat or cold work is applied to the specimen. Cross-section samples were then mounted in Bakelite and polished to 3µm. The final polishing step for EBSD preparation was a 30-minute polish with a 0.04µm colloidal silica solution. EBSD data was collected using a Hitachi SU3000 tungsten filament SEM utilising an Oxford Nordlys EBSD detector. A 200µm x 200µm area with a step size of 0.5µm was mapped, whilst ensuring the material surface was captured. Analysis of the ESBD data was conducted using HKL Channel 5 software. Local pattern averaging was applied using 11 nearest neighbours to define the misorientation map.

Finally, in order to verify the results generated and explore the possibility of increased stress intensity due to pit geometry, the stress fields around the pits were analysed using the commercially available finite element analysis software, ABAQUS. The profile of two typical pits

(110H and 330H) were obtained from SEM images and stress was applied by means of a prescribed displacement (Dirichlet boundary condition) to give an equal nominal stress across the narrowest cross section. The stress intensity was then calculated by dividing the maximum predicted stress at the pit by the nominal stress.

2.2. Salt Application

To generate the required hot corrosion and high temperature corrosion-fatigue morphology within the laboratory, salt must initially be applied to the specimen prior to exposure.

Within the HP turbine, salt is present via the ingestion of sea salt along with the presence of sulphuric gases; a bi-product of the combustion process. In service, the salt is deposited on turbine components in a stochastic, globular manner and reacts at elevated temperatures to form molten sulphate deposits which can attack the protective surface oxides resulting in Type II hot corrosion, demonstrated by Equation 3, as well as isolated pitting [15].

$$2NaCl + SO_3 + O_2 = Na_2SO_4 + Cl_2 \qquad \text{(Equation 3)}$$

A technique has been developed specifically for this role, where a salt solution consisting of 98%Na_2SO_4 – 2%NaCl combined with 45% MeOH and 55% H_2O is prepared [16]. The specimen is pre-heated on a hotplate (or heated turntable for round-bar samples) to a temperature of 100°C and monitored using a calibrated N-type thermocouple and Fluke-meter. The solution is applied directly to the specimen surface utilising a fine-nozzle spray gun controlled by a timed pneumatic actuator. The salt spray settings are optimised such that a service-representative salt deposition is achieved, similar to that observed in Figure 3. Obtaining a stochastic salt deposition is essential in generating isolated pitting as opposed to broad-front, uniform attack. Preliminary studies determined that a flux level of 0.15mg/cm^2 (+/- 0.01mg/cm^2) provided hot corrosion and corrosion-fatigue morphologies akin to in-service damage. The procedure and parameters used for salting flat plates was analogous to that used for round bars.

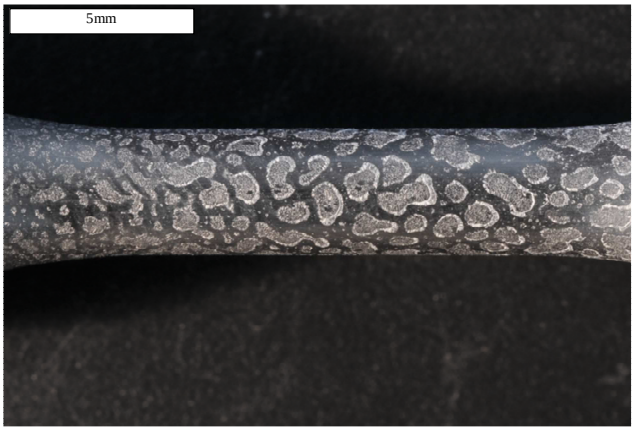

Figure 3 – Visual representation of optimised salt distribution, utilising spray gun with 98%Na_2SO_4 – 2%NaCl based solution.

2.3. Fatigue Assessment

Two sets of fatigue tests were carried out: high temperature air fatigue for baseline analysis and high temperature corrosion-fatigue tests to assess the influence of a corrosive environment.

All tests were carried out utilising a 100kN Instron servo-hydraulic test frame and a radiant furnace capable of heating the sample to 700°C. The fatigue loading cycle consisted of a 6-second triangular waveform, to minimise the effect of creep during dwell times, at an R=-1 with a fixed intermediate stress level, suitable for the material, to simulate the typical cyclic loading conditions witnessed by the turbine disc. A total of three repeat tests per surface condition were carried out and all specimens were tested to failure.

Where high temperature corrosion-fatigue testing was carried out, the fatigue load train was encapsulated by an environmental test chamber and surrounded by a radiant furnace. The chamber, and thus the sample, is heated to a temperature of 700°C whilst being exposed to an inert gas before introducing the fatigue cycle. This prevents the formation of low melting point eutectics forming at transient temperatures, the growth of any potentially protective, non-representative oxides and allows for full control of the test. Once maximum temperature is reached and stabilised, a continuous flow of 80mln/min air – 300ppm SO_2 is activated and the fatigue loading profile is started. When the sample fails, similarly to the heating process, the chamber is cooled under inert gas exposure until at room temperature.

2.4. Hot Corrosion Testing

In order to gain a further understanding of the mechanisms that occur under corrosion-fatigue conditions, hot corrosion testing (without stress) was carried out to remove the effect of fatigue. Testing was carried out on 6 RR1000 flat plate specimens, 3 of each surface condition; 110H and 330H shot size. The pre-salted samples were placed within a static environmental test chamber, similarly described in section 2.3. Once at temperature, the SO_2 gas is activated and a test duration of 50 hours is timed. This is a suitable time to generate representative corrosion damage.

3. Results

3.1 Baseline Material Analysis

Values of S_a and R_a for 110H and 330H prior to testing are contained in Table 2. Figures 4a and 4b show a 4x4mm region of the surface represented three-dimensionally.

Surface Condition	Roughness (Sa)	Roughness (Ra)
Polished	0.536	0.514
110H 7A 200%	1.35	1.26
330H 7A 200%	1.13	1.01

Table 2 - Surface roughness measurements for various shot size conditions for a 4x4mm mapped area.

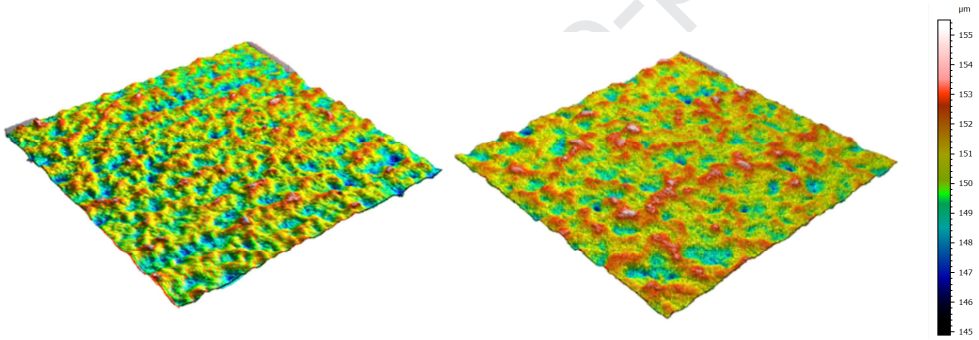

Figure 4 – Three-dimensional representations of untested shot peened surfaces constructed via axial chromatism (a) 110H, (b) 330H.

Figure 5 shows the local misorientation maps of the near surface region of the untested samples of all three surface finishes; (a)polished (b)110H and (c) 330H. The low angle range of 0°-1.4° is represented by a blue (0°) and green (1.4°) colour scale within all EBSD maps.

(a)

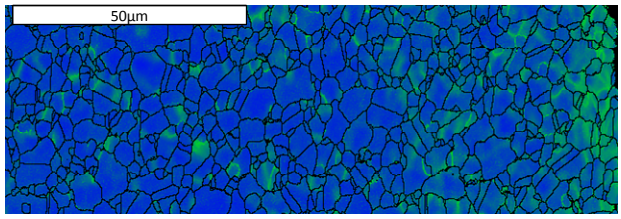

(b)

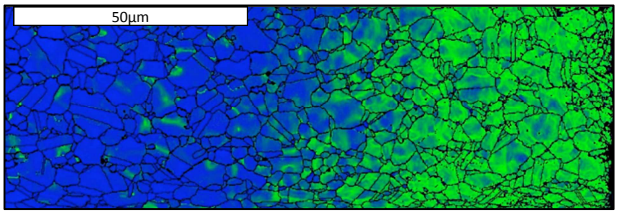

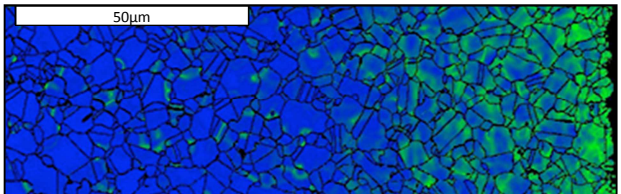

(c)

Figure 5 – Local misorientation maps of (a) polished surface (b) 110H shot size (c) 330H shot size

3.2 Fatigue Assessment

Figure 6 illustrates the average fatigue life for all surface conditions under both air and corrosion fatigue at 700°C at a fixed stress amplitude. Error bars illustrate the approximate scatter witnessed within the data.

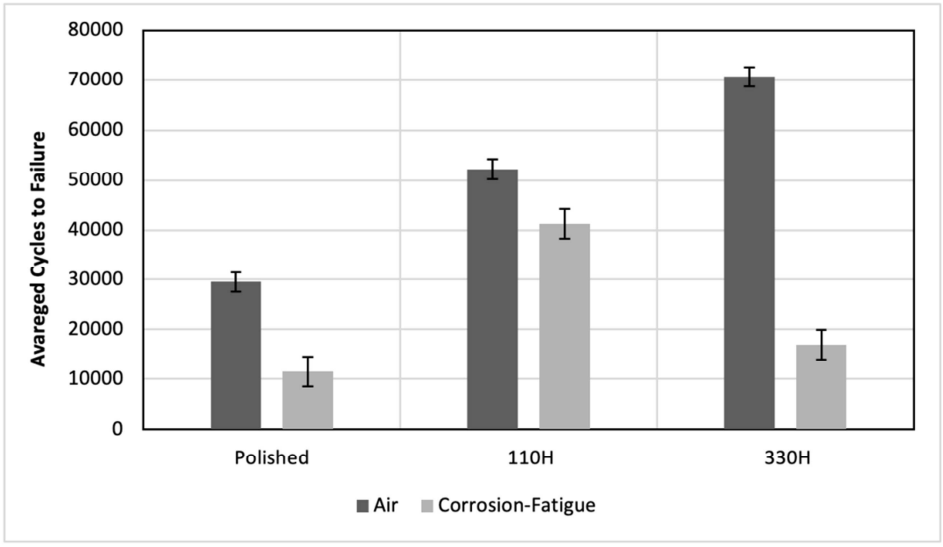

Figure 6 – RR1000 averaged fatigue data produced at 700°C in air and in a corrosive environment at fixed intermediate stress amplitude, R=-1, 6-second triangular waveform. Comparison of different surface conditions; polished, 110H and 330H shot size.

Table 3 quantifies the decrease in fatigue life in terms of percentage, when comparing air-fatigue to corrosion-fatigue.

Surface Condition	% decrease in Fatigue life
Polished	61
110H 7A 200%	21
330H 7A 200%	76

Table 3. % decrease in fatigue life from air when tested in a corrosive environment.

EBSD analysis was carried out utilising the techniques discussed previously, for corrosion-fatigue samples and results are shown in Figure 7, where surface finishes were (a) polished, (b) 110H shot size and (c) 330H shot size.

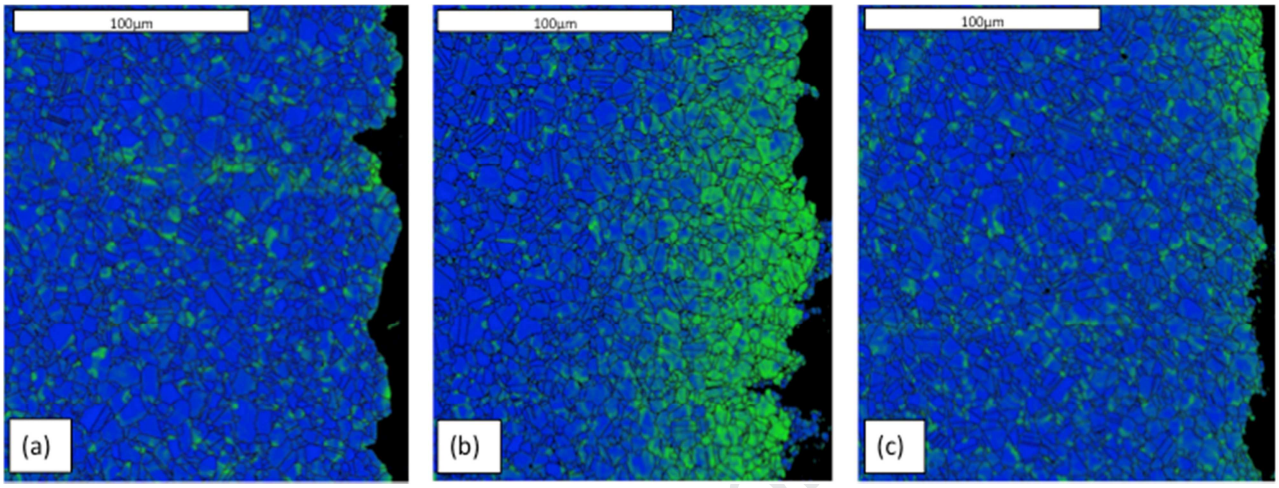

Figure 7 – Local misorientation EBSD maps for corrosion-fatigue tested samples of various surface conditions (a) polished, (b) 110H (c) 330H

3.3 Hot Corrosion

Hot corrosion samples were also analysed via the EBSD KAM method described in Section 2.2. Figure 8 shows a comparison of 110H and 330H samples in the untested and tested condition. Highlighted are the regions of near-surface cold work, represented by the low angle misorientation, as 75 µm and 25µm, respectively.

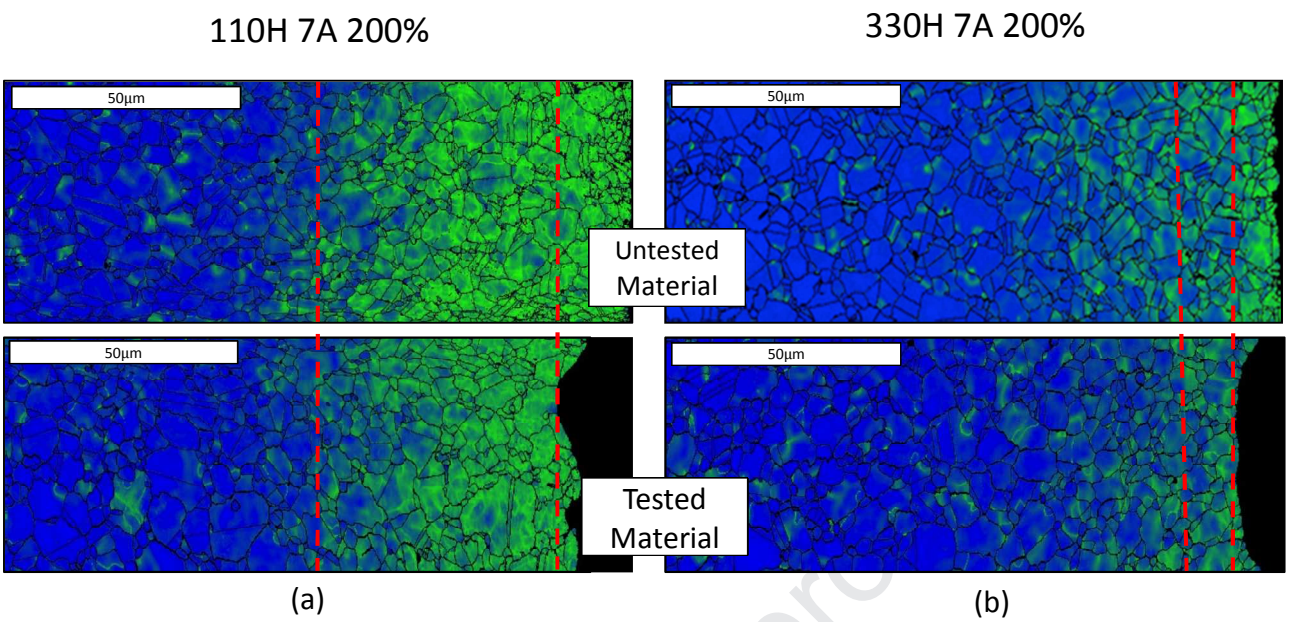

Figure 8 – Local misorientation maps detailing the cold work at the surface of the specimens before and after hot corrosion testing for (a) 110H and (b) 330H.

Typical examples of corresponding 3D surface profiles are also provided for both post-test hot corroded samples in Figure 9.

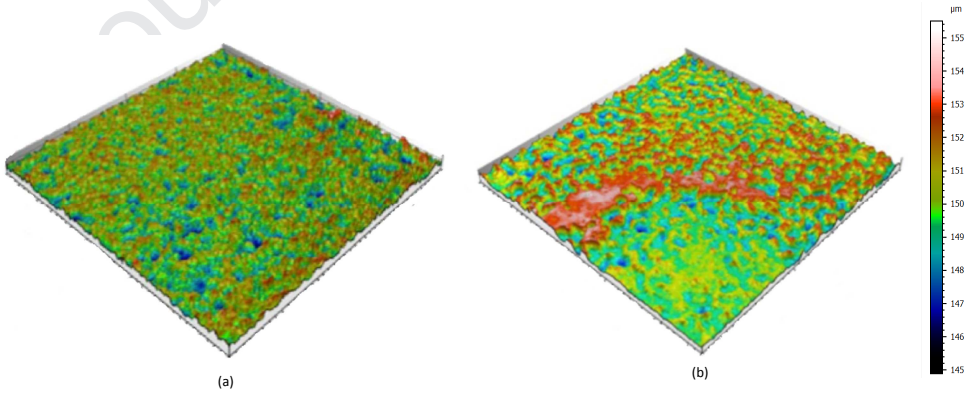

Figure 9 – 3D surface profiles for (a)110H and (b)330H tested in a hot corrosion environment

In addition, Figure 10 shows the pit density per unit area vs pit depth for both peening conditions before and after hot corrosion testing. It must be noted that when 'pits' are referred to in the pre-test condition, the values represent the indents associated with shot peening.

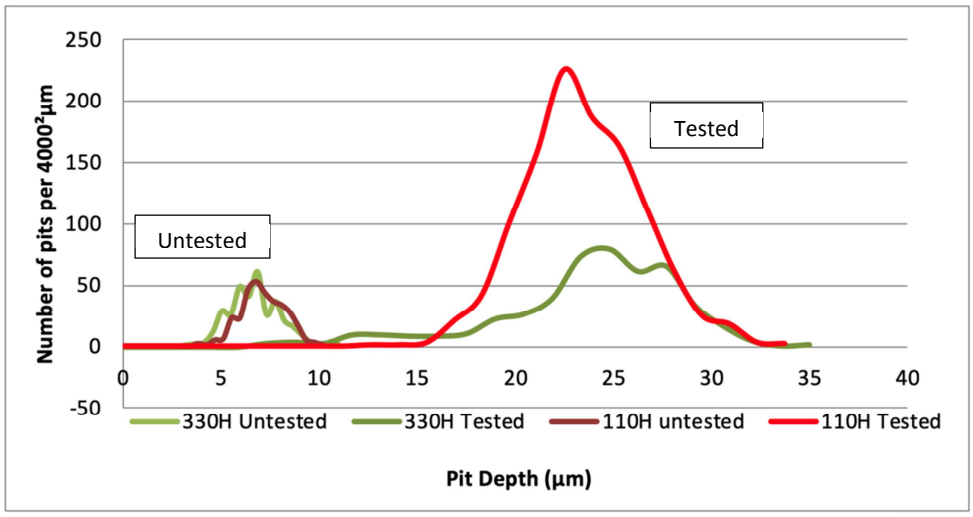

Figure 10 – Number of pits vs pit depth for tested and untested 110H and 330H specimens

The stress intensities at an average sized pit in both the 110H and 330H specimen are shown in Figure 11.

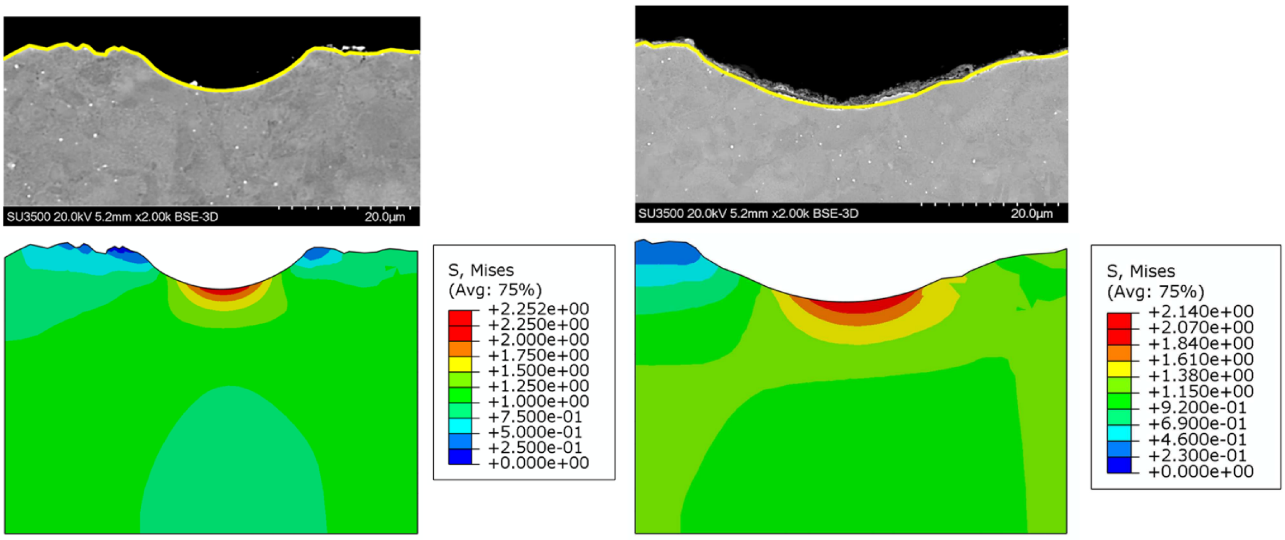

(a) (b)

Figure 11- FEA of an average size pit from (a) 110H specimen (b) 330H specimen

4. Discussion

A comparison of R_a against S_a results shows little variability and therefore S_a has been used to provide a more detailed assessment of the pre and post-corroded surface as well as 3D representations. As expected, the polished finish displays the lowest surface roughness (S_a)

followed by the 330H and the 110H shot size. The larger radius of the 330H shot results in a wider shaped indent compared to the 110H, even when the same intensity is used, and subsequently results in a smoother surface and a resulting lower S_a value. This correlates with Hertzians' theory of non-adhesive elastic contact, where a spherical body, with a parabolic pressure profile comes into contact with a continuous half-space. The body with a radius (R) and contact force (F) generates an indentation of depth (u), which is given by Equation 4 [17].

$$u \cong \left(\frac{2F^2}{E_*^2 R}\right)^{1/3}$$

(Equation 4)

where E_* is related to the sum of elastic moduli and the Poisson's ratios associated with each body. This equation surmises that for a fixed shot intensity, when the radius of the shot is increased, the resulting indent will typically be broader and shallower in geometry. Hertzians' theory has also been applied to the generation of sub-surface residual stresses and localised deformation and has yielded comparable results to Finite Element modelling and experimental photo-elastic work. [18]

In order to quantify the depth of this localised deformation, or plastic strain, EBSD techniques have grown in popularity in recent years, with many different methods being utilised, including grain orientation spread (GOS) and KAM [19][20]. Authors have shown good consistency with other techniques such as hardness testing and X-Ray Diffraction. Within this study, this technique has been effectively used to illustrate the effects of the different shot peening parameters and how the magnitude of the corrosive attack can influence the depth of the strain hardened layer. It is evident from the local misorientation images shown in Figure 5, that shot peening and shot size can influence the level of near-surface plastic strain within the material. Figure 5a shows a negligible amount of misorientation due to the lack of imparted cold work whereas Figure 5b shows that a 110H shot size imparts a consistent strain hardened layer with an average depth of 75μm; and Figure 5c shows a depth of 25-35μm for a 330H shot size. It is understood that the initial levels of residual stress imparted by the 110H and 330H shot are of similar magnitude and depth and when exposed to stress and/or temperature, would be expected to relax in a consistent manner.

The combination of fatigue cycles and high temperature would be expected to reduce the residual stress to levels where they do not significantly affect the trends in the current work and results shown within this paper appear to show a stronger correlation with findings from the strain hardened layer and surface roughness.

In order to fully understand the effect of surface finish on the fatigue response of fine grain RR1000 in a corrosive environment, it is essential to first consider the effects under air fatigue. When analysing the air-only data, it is clear that shot size, and thus near-surface plastic strain, as the only varying factor, has a large influence on fatigue performance. It is observed that the fatigue life in air is seen to increase as the shot size is increased and the effect is particularly visible when comparing polished to shot peened specimens, where a significant increase in fatigue life is observed when a layer of cold work is introduced at the surface. The lack of cold work present at the surface of the polished samples, combined with a poor fatigue life, suggests that the presence of a cold work layer is a key factor in enhancing the high-temperature fatigue performance in fine grained RR1000 in air. It is believed that the residual stress at the surface will also likely contribute to this benefit initially. It also appears that the surface roughness has an effect on fatigue initiation in this case, with the 330H outperforming the 110H samples, with an approximate life extension of 30%. Although variations in surface roughness are seen to be small, RR1000 has shown to be particularly sensitive to surface roughness and initiation, which has been explored in depth by Ardi *et al* [21]. The increase in S_a for 110H shot peened samples has also been seen to be accompanied by mechanical surface features, such as laps, folds and indents which could also increase the potential of early surface initiation. [22]

When a corrosive environment is introduced, the data analysed in Figure 6 shows an as-expected overall decrease in fatigue life, across all surface finishes. The data shows that the 110H shot size offers the best corrosion-fatigue response of the peened conditions with the 330H experiencing a drastic decrease in fatigue life, with an almost similar life to those of un-peened and polished samples. As in air, the polished specimens demonstrate the poorest fatigue performance, suggesting a strain hardened surface is still required to improve fatigue resistance. Under corrosion-fatigue conditions, the 330H shot size exhibits the largest decrease in fatigue performance, with a reduction percentage of 76.01% in cycles to failure. The 110H shot size on the other hand, demonstrates a much smaller fatigue life reduction of 21.15%, when exposed to a corrosive environment, and thus providing the best performance under such conditions. When the extent of the post-test strain hardened layers shown in Figure 7 are considered, the substantial decrease in fatigue life observed in the 330H specimens becomes apparent.

Figure 7a highlights, that in terms of low angle misorientation, there is no plastic strain present in the polished sample, as expected, and as shown in the baseline material analysis, Figure 5a. This lack of near-surface plastic strain is also paired with distinct surface features that would likely cause or accelerate initiation. When comparing Figures 7b (110H) and 7c (330H), the

110H sample exhibits a considerable amount of plastic deformation near the surface as opposed to the 330H sample, where there is little to no cold worked material remaining. The EBSD results suggest that despite 110H showing a higher surface roughness and pit density (shown in Figure 10), meaning that early crack initiation would be expected, as witnessed by Gallo *et al* [23], the surface roughness is outweighed by the presence of an extensive layer of cold work. When analysing the corrosion-fatigue samples for the 110H condition, the majority of corrosion damage, which includes pitting, channelling, metal loss and fissures, was contained within the layer of cold-work. The corrosion-fatigue life for a 110H shot peened sample is therefore substantially extended. Specimen failure occurs when the crack grows to a critical length and exceeds the fracture toughness of the alloy. The 330H condition exhibits this effect, with little to no remaining strain hardened layer, resulting in a reduced pit-crack transition time. It was observed, however that metal loss in the 110H specimens was greater than that in the 330H specimens. This is likely to be attributed to test time; due to the large reduction in life experienced by the 330H condition, the 110H specimens were exposed to the corrosive environment for a longer time duration. This allowed for corrosive, time-dependent mechanisms to take place, which typically results in broad front attack and greater rates of corrosion [24].

When the specimens are hot corroded, and the effect of stress is isolated, a marked increase in pit depth and density is observed for the 110H condition, as shown in Figure 10, where the pit density increases to ≈ 225 pits per 4x4mm area and the average pit size increases to ≈ 22μm. The pit density for the 330H peeing conditions shows a slight increase in pit density up to ≈ 76 pits per 4x4mm area and an increase in pit depth with an average of ≈ 25μm. This highlights that the surface roughness alone has an effect on the pitting propensity of RR1000, where a rougher surface is likely to exhibit higher rates of corrosion and a higher frequency of associated pitting.

When FEA analysis was conducted of two typical hot corrosion pits in a 110H and a 330H shot peened sample, as shown in Figure 11, the stress intensity in the 110H specimen is slightly higher due to the aspect ratio of the pit. Stress intensities of K_t = 2.25 were calculated for the 110H specimen and K_t = 2.14 for the 330H specimen, shown in Figures 11a and 11b respectively. However, under operating conditions, non-linear deformation such as creep and plasticity will occur which would relax the stress at these features resulting in a more homogenised sub-surface stress. Despite having a higher geometric stress concentration factor, a higher frequency of pitting, higher surface roughness *and* suffering more metal loss within a corrosive atmosphere, the 110H shot peened samples demonstrated a significantly better high

temperature corrosion-fatigue response. It is believed that the only varying factors within this study are the roughness of the surface and the depth of plastic deformation. In the case of the 110H sample, the depth of plastic deformation provided by the smaller shot size, remains present within the samples after corrosion-fatigue or hot corrosion has taken place and is thus clearly a factor in hindering crack formation and propagation.

5. Conclusions

- A Kernal Average Misorientation (KAM) approach has been used to generate low angle misorentation EBSD maps in order to quantify the depth of the strain hardened layer due to shot peening in a nickel-based superalloy, both pre and post corrosion-fatigue and hot corrosion testing. By utilising the KAM method, it has been shown that 110H shot size produces a 75 μm cold work layer and 330H shot size produces a 25μm layer.
- Axial chromatism has been utilised to determine surface roughness in terms of both R_a and S_a, as well as provide 3D surface representations and pit density before and after exposure to a corrosive environment. 110H shot size exhibits a higher surface roughness and pit density when compared to 330H shot.
- Under air-only fatigue conditions, the presence of cold work due to shot peening is shown to be a benefit, when compared to un-peened, polished material. A low surface roughness will also improve the fatigue response of a material, as expected. Both a good surface roughness and a sufficient layer of cold work is provided by a 330H shot size and thus provides the best fatigue response in air.
- Under corrosion-fatigue conditions, 110H shot size shows a significant life benefit. Despite having a higher surface roughness, greater pit density, higher geometric pit concentration factor and greater metal loss, the 110H shot provides a substantial layer of cold work, thus appearing to hinder the transition from pit to crack.
- When the presence of a corrosive environment is introduced, time dependent and stress-induced surface effects such as metal loss and pitting can result in complete removal of the strain hardened layer. In the case of the 330H shot peened samples, which has a comparatively small layer of cold work, the metal loss has penetrated and exceeded the depth of this layer and resulted in a considerable reduction in fatigue life, similar to that of un-peened specimens.
- The results therefore indicate that a combination of a deep cold worked layer and a low surface roughness would be required to optimise the fatigue performance in both air and a corrosive environment.

Acknowledgements

This work was supported by the Aerospace Technology Institute (Innovate UK) under SILOET II P17 – High Temperature Nickel Alloy, project 113018.

References

1. F. Petit, Hot corrosion of metals and alloys, Oxid Met 2011;76:1-21.
2. K.L. Luthra, Low temperature hot corrosion of cobalt-base alloys: part II. Reaction mechanism. Metallurgical Transactions A, 1982:18(10): 1853-1864.
3. G.Lai, High-temperature corrosion and materials applications, ASM International, 2007.
4. R.Viswanathan, An investigation of blade failures in combustion turbines, Engineering Failure Analysis, 2001:8:493-511.
5. H.L.Cockings, K.M.Perkins, M.Dowd, Influence of environmental factors on the corrosion-fatigue response of a nickel- based superalloy, Materials Science and Technology, 2017:33:9:1048-1055.
6. B.Foss, S.Gray, M.C.Hardy, S.Stekovic, D.S McPhail *et al,* Analysis of shot-peening and residual stress relaxation in the nickel-based superalloy RR100, Acta Materialia, 2016:61:2548-2559.
7. A., Evans, S-B.Kim, J.Shackleton, G.Bruno, B.Giovanni *et al,* Relaxation of residual stress in shot peened Udimet 720Li under high temperature isothermal fatigue, International Journal of Fatigue, 2005: 27: 1530-1534.
8. G.Gibson, K.M.Perkins, S.Gray, A.J.Leggett, Influence of shot peening on high temperature corrosion and corrosion-fatigue of nickel based superalloy 720Li, Materials at High Temperatures, 2015:33(3):225-233.
9. J.D Ramsey, H.E.Evans, D.J.Child, M.P.Taylor, M.C.Hardy, The influence of stress on the oxidation of a Ni-based superalloy, Corrosion Science, 2019:154:277-285.
10. SAE International, AMS2432, Computer Monitored Shot Peening.
11. ISO (2014) 16610-71:2014 Geometrical product specification – Filtration. Part 71: Robust areal filters: Gaussian regression filters.
12. Y.Quinsat, L.Sabourin, C.Lartigue, Surface topography in ball end milling process: Description of a 3D surface roughness parameter, Material Processing Technology, 2008:195(1-3):135-143.
13. M.Kamaya, Assessment of local deformation using EBSD: Quantification of local damage at grain boundaries, Materials Characterisation, 2012:66:56-67.
14. M.Kamaya, Characterisation of microstructural damage due to low-cycle fatigue by EBSD observation, Materials Characterisation, 2009:60:1454-1462.
15. N.Eliaz, G.Shamesh, R.M.Lataniston, Hot corrosion in gas turbine components, Engineering Failure Analysis, 2002:9(1):31-43.

16. H.L.Cockings, K.M.Perkins, S.Gray, Optimisation of a salt deposition technique for the corrosion-fatigue testing of nickel based superalloys, Materials at High Temperature, 2018:35(5):451-460.
17. K.L.Johnson, Contact Mechanics, Cambridge University Press, Cambridge, 1985.
18. S.Kyriacou, Shot peening mechanics: a theoretical study, 6th International Conferences on Shot Peening, 1996, 505-516.
19. K.A.Soady, B.G.Mellor, G.D.West, G.Harrison, A.Morris, P.A.S.Reed, Evaluating surface deformation and near surface strain hardening resulting from shot peening a tempered martensitic steel and application to low cycle fatigue, International Journal of Fatigue, 2013:54:106-117.
20. D.J.Child, G.D.West, R.C.Thomson, Assessment of surface hardening effects from shot peening on a Ni-based superalloy using electron backscatter techniques, 2011:59(12):4825-4834
21. D.Ardi, 2014, The effect of surface topography on the life of critical gas turbine components, PhD thesis, Swansea University.
22. R.L.Barrie, T.P.Gabb, J.Telesman, P.T.Kantzos, A.Prescenzi, T.Biles, P.J.Bonacuse, Effectiveness of shot peening in supressing fatigue cracking at non-metallic inclusions in Udimet 720, 2006, NASA Technical Reports, Number NASA/TM-2005-213577, E-15044.
23. P.Gallo, F.Berto, Influence of surface roughness on high temperature fatigue strength and crack initiation in 40CrMoV13.9 notched components, Theoretical and Applied Fracture Mechanics, 2015:80:226-234.
24. A.P.Gordon, M.D.Trexler, R.W.Neu, T.J.Sanders, D.L.McDowell, Corrosion kinetics of a directionally solidified Ni-based superalloy, Acta Materialia, 2007:55(10):3375-3385.

Highlights

- Compressive residual stress due to shot peening is not the only benefit provided to material surfaces. Cold work (or plastic deformation) provides benefit in terms of corrosion resistance at high temperatures, as well as fatigue.
- Levels of cold work are found to vary significantly by changing peening variables such as shot size. Cold work can be characterised using electron backscatter diffraction methods.
- A combination of a low surface roughness and a deep level of cold work enhanced the performance of a nickel based superalloy under high temperature corrosion-fatigue conditions.

Declaration of interests

☒ The authors declare that they have no known competing financial interests or personal relationships that could have appeared to influence the work reported in this paper.

☐The authors declare the following financial interests/personal relationships which may be considered as potential competing interests: